SUPPORTING INFORMATION MATERIAL

Dynamic Surface Processes of Nanostructured Pd_2Ga Catalysts Derived from Hydrotalcite-Like Precursors

Antje Ota[†], Jutta Kröhnert[†], Gisela Weinberg[†], Igor Kasatkin[†], Edward L. Kunkes[†], Davide Ferri[†,††], Frank Girgsdies[†], Neil Hamilton[†], Marc Armbrüster[‡], Robert Schlögl[†], Malte Behrens[†,*]

[†] Fritz-Haber-Institute of the Max-Planck-Society, Department of Inorganic Chemistry, Faradayweg 4-6, 14195 Berlin, Germany

[††] Paul Scherrer Institut, 5232 Villigen, Switzerland

[‡] Max-Planck-Institut für Chemische Physik fester Stoffe, Nöthnitzer Strasse 40, 01187 Dresden, Germany

*E-mail: behrens@fhi-berlin.mpg.de, Phone: +49 30 8413-4408, Fax: +49 30 8413-4405

Supporting Information includes further discussions and additional experimental details as well as a precipitation protocol (Figure S1), XANES spectra of reference PdZnAl HT sample (Figure S2), XRD patterns of the HTlc precursors (Figure S3) and their evaluation (Table S1), SEM micrographs and EDX line scans of the HTlc precursors (Figure S4) and additional micrographs in the BSE mode of Pd10 and Pd25 (Figure S5), MS data of the TPR experiments (Figure S6), XRD powder pattern of the catalysts after reduction (Figure S7), HRTEM images of selected Pd_2Ga particles (Figure S8), IR spectra of CO adsorbed on Pd10 in OH stretching region (Figure S9), additional IR spectra of adsorbed CO (Figure S10), CO chemisorption results (Figure S11), Conversion and selectivity at 473 K over Pd25 (Figure S12), an Arrhenius plot to determine the apparent activation energy (Figure S13), Raman spectra of Pd_2Ga25 before and after reaction (Figure S14) and TPO of Pd25 after 44h time on stream (Figure S15). This material is available free of charge via the Internet at http://pubs.acs.org.

Experimental Details regarding the data presented in the supporting information:

Scanning electron microscopy (SEM) images were acquired with a Hitachi S4800 FEG microscope equipped with an EDS system (EDAX Genesis with Si(Li) detector) for elemental analysis. The samples were loosely dispersed on a conductive carbon tape to preserve the as-prepared morphology as much as possible.

X-ray diffraction (XRD) patterns of the HTlc precursor and its decomposition products were recorded on a STOE Stadi P diffractometer in transmission geometry using Cu $K\alpha_1$ radiation, a primary Ge monochromater and a 3° linear position sensitive detector.

Evolved gas during TPR was analyzed using a quadrupole mass spectrometer (QMS200 Omnistar, Balzers).

The volumetric CO adsorption measurements were carried out in an Autosorb 1C (Quantachrome Instruments). The samples were pretreated in-situ in the sample cell by heating to 500 °C K for 240 min in 5% hydrogen in helium flow (20 ml/min), followed by an evacuation (240 min) at pretreatment temperature. CO chemisorption measurement was performed at 40°C and in the pressure range of 2 - 560 Torr.

Discussion of hydrogenation on Pd surfaces (taken from [1]):

The fundamental mechanism of acetylene and ethylene hydrogenation following the Horuiti-Polanyi mechanism[2] was studied by DFT calculations on a clean Pd(111) surface[3,4]: acetylene and ethylene are converted by subsequent half-hydrogenation with vinyl and ethyl, respectively, as intermediates on the surface, which requires ensembles of Pd atoms. Azad et al.[5] determined the acetylene hydrogenation to vinyl as rate limiting step as detected by joint TPD and IR absorption measurements on Pd(111) under UHV conditions. Ethylidyne was detected after heating the surface above 160 K.

Generally, alkynes are adsorbed stronger than alkenes. An early explanation for the high selectivity of Pd was a strong thermodynamic factor, meaning that as long as an alkyne is present the alkene is displaced from the surface. However, it is well-known that Pd-based catalyst can operate in a selective as well as in an unselective manner favoring formation of the alkene and alkane respectively. Bond and Wells[6] showed that the selectivity of Pd for acetylene hydrogenation decreases as the initial H_2 : acetylene ratio increases and at sufficiently high ratios the reaction becomes completely non-selective. It was shown furthermore, that acetylene and ethylene can be indeed adsorbed and hydrogenated simultaneously and ethylene hydrogenation proceeds faster than the acetylene hydrogenation[7]. The formation of oligomers and carbonaceous deposits due to dissociative adsorption are additionally observed side reactions. In particular ethylidyne, but also other intermediates resulting from dissociative adsorption like vinylidene or acetylide, are intermediates that have been observed in various studies[8,9]. They were suggested to be precursors for carbonaceous deposits as well as oligomers.

Sample identification

HTlc precursors:		After HTR:	
Label	*FHI internal sample number*	*Label*	*FHI internal sample number*
Pd0	11369	Pd_2Ga0	11754
Pd01	10198	Pd_2Ga01	12462
Pd03	10199	Pd_2Ga03	12419
Pd05	10200	Pd_2Ga05	12385
Pd08	10201	Pd_2Ga08	12423
Pd10	10230	Pd_2Ga10	11121
Pd15	10231	Pd_2Ga15	12390
Pd25	10232	Pd_2Ga25	11782

To facilitate communication and sample assignement, please refer to these electronic database numbers upon correspondence.

Synthesis protocol

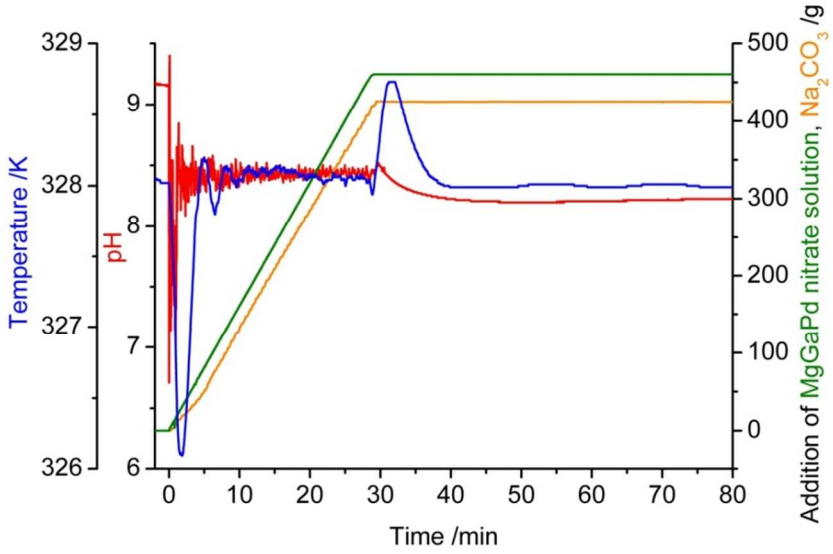

Figure S1: Synthesis protocol of Pd15 HTlc precursor.

PdZnAl HTlc as reference compound for octahedral Pd^{2+}

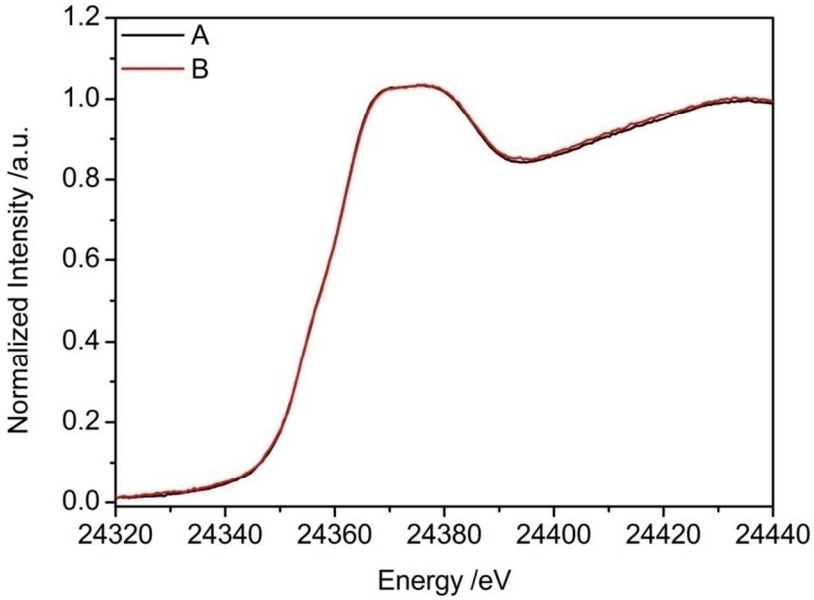

Figure S2: XANES spectra of PdZnAl HT at RT in (A) Helium and (B) 5 Vol% H_2/He.

No change of the white line was observed upon feeding hydrogen over the PdZnAl HT reference sample with 1 mol% Pd at RT. This assumes that Pd^{2+} is completely incorporated into the HTlc lattice and not available for reduction at room temperature. Accordingly, no RTR H_2 consumption was observed-Thus, we conclude that PdZnAl HT can be used as reference for octahedrally coordinated Pd^{2+} in HTlc.

Synthesis: PdZnAl HTlc were synthesized by controlled co-precipitation at pH = 8.5 and a temperature of 298 K by co-feeding appropriate amounts of mixed metal nitrate and mixed sodium hydroxide/sodium carbonate solutions(0.045 M Na_2CO_3 + 0.3 M NaOH). The following synthesis steps are equal to the herein presented synthesis protocol. The experimentally determined Pd:Zn:Al atomic ratio was 1:69.5:29.5.

XRD results of HTlc precursors:

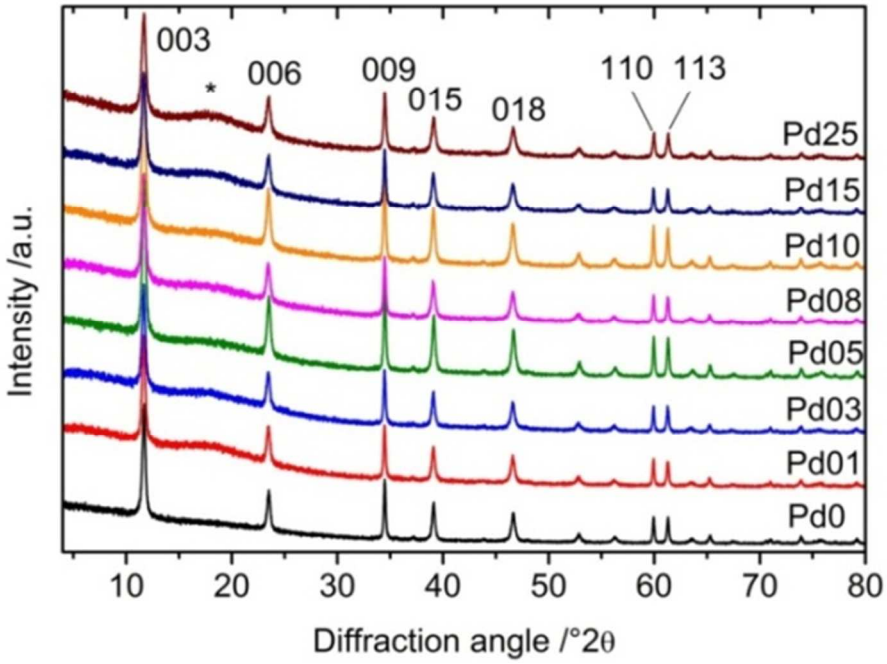

Figure S3: XRD patterns of the MgGa HTl precursor with different Pd loadings (*sample holder).

The XRD patterns of the precursors indicate a high crystallinity and single-phase HTlc structure. No crystalline Pd containing byphase was observed up to a Pd loading of 2.5 mol%. By Rietveld refinement (not shown) the lattice parameters were determined and are reported in Table S1. For Pd0 the calculated *a* and *c* parameter of 3.087 Å and 22.7 Å, respectively, are close to those reported in literature.[20] Lopéz et al. [20a] varied the Mg:Ga ratio from 12.9-1.8 in their studies and observed a linear decrease of the *a* parameter (3.123 - 3.086 Å), indicating that smaller Ga^{3+} cations are incorporated into the layered structure to a variable extent. Also the interlayer spacing, related to the *c* parameter, shrinks (24.52 - 22.72 Å) as the Ga content increases, due to a greater electrostatic attraction between layers and interlayers. The lattice parameters of the Pd substituted samples are similar to those of the unsubstituted precursor and do not show a trend with the Pd content. This suggests that the amount of Pd^{2+} incorporated into the HTlc is low or that substitution of Mg^{2+} by Pd^{2+} has little impact on the structure although Pd^{2+} exhibits a larger ionic radius (0.86 Å [18]). However, no reliable conclusion about Pd incorporation in the investigated compositional range can be drawn from the XRD results.

Table S1: Lattice parameter and peak width of the precursor samples.

Sample	Lattice parameters[a]		FWHM
	a [Å]	*c* [Å]	003 [°2□]
Pd0 HT	3.087	22.740	0.224
Pd01 HT	3.087	22.763	0.325
Pd03 HT	3.087	22.778	0.331
Pd05 HT	3.086	22.721	0.347
Pd08 HT	3.086	22.778	0.379
Pd10 HT	3.087	22.755	0.374
Pd15 HT	3.087	22.769	0.393
Pd25 HT	3.085	22.753	0.421

[a] Uncertainty approx. ±0.003 and ±0.06 Å for *a* and *c*, respectively; [b] Pd content after reduction at 773 K

SEM-EDX results:

Typical plate-like particles were obtained for all samples and the platelets are approximately 1 µm in diameter and the thickness is in the order of 5-20 nm (Figure S2a). Elemental mapping (not shown) revealed a homogenous metal distribution within the resolution of the method and no Pd-rich agglomerates were observed. In case of the 1 mol% Pd sample an EDX line scan of the Mg K-, Ga L- and Pd L fluorescence lines displayed a homogenous metal distribution for all three metal species within a larger aggregate (Figure S4b). With this method, Pd-rich areas were observed for 1.5 mol% and 2.5 mol% Pd loadings (Figure S2c) suggesting that either the upper limit for the incorporation of Pd into the HTlc layers is < 1 mol% or that the detection limit of the method is reached due to the low total amount of Pd in the sample Pd10. The inhomogeneous metal distribution in the Pd-richer samples was confirmed by contrast fluctuations in the backscattering electron (BSE) microscopy image (Figure S3).

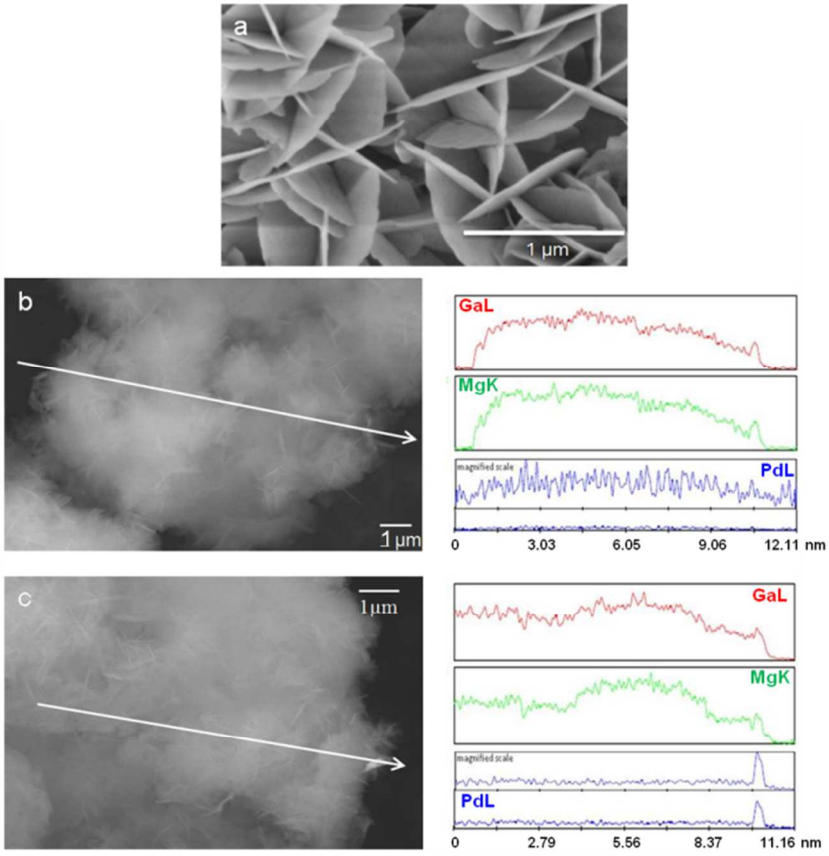

Figure S4: (a) SEM micrographs of Pd10 (recorded V_{acc}=2kV), EDX line and micrographs of (b) Pd10 and (c) Pd25 (recorded at V_{acc}=15kV)

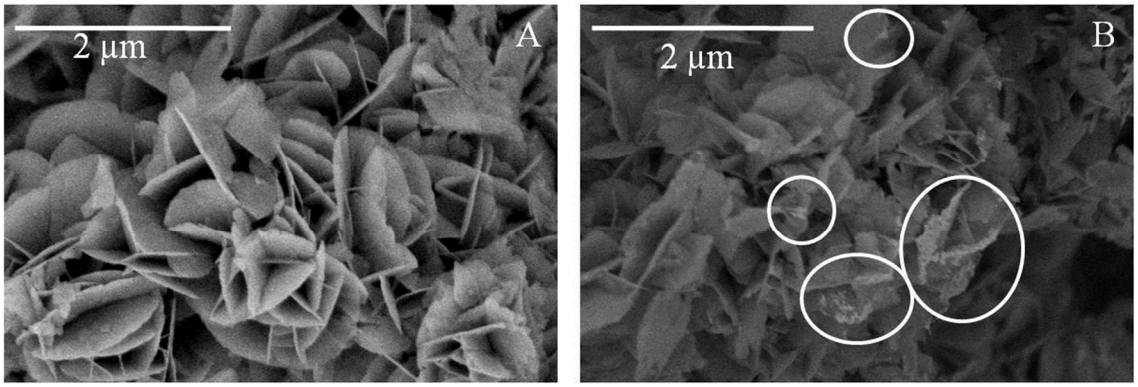

Figure S5: BSE images of Pd10 (A) and Pd25 (B). Enhanced contrast allows the identification of Pd rich areas outside the platelets in the latter sample (recorded with V_{acc} = 2 kV).

MS data of the TPR experiments:

The profiles of mass signals m/e = 15, 18, 28 and 44 observed during reduction in hydrogen are shown in Figure S6 for Pd0, Pd10 and Pd25. At the beginning of the experiment mainly water (m/z = 18) is released from the interlamellar space. A maximum is observed at 448 K for all samples. Simultaneously, labile carbonate ions decompose into CO_2 (m/z = 44) and are observed in small quantities.

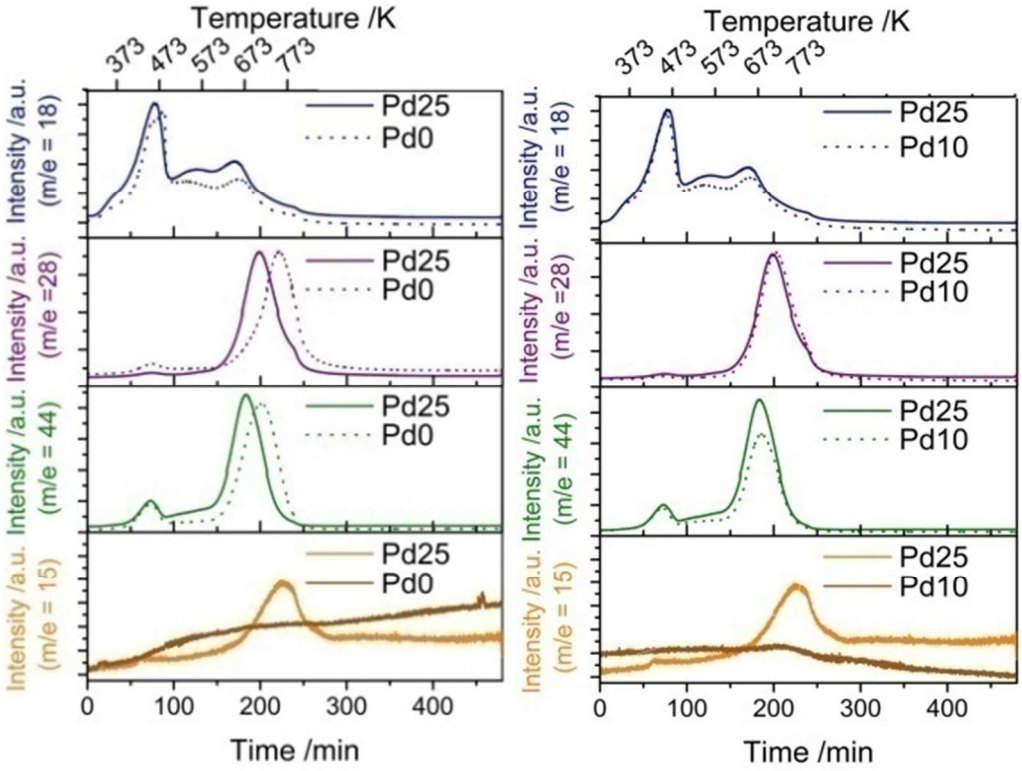

Figure S6: Mass signals during thermal decomposition and reduction of Pd0, Pd10 and Pd25 HTlc in 5 Vol% H_2/Argon (heating rate 2 K/min).

Upon heating to 773 K additional water evolution is detected and levels off during temperature holding. The release of water is related to the dehydroxylation of the brucite-like layers. CO_2 release starts around 573 K and result from decarboxylation of the interlayer space which is usually observed during thermal treatment for HTlc.[23] Shortly thereafter CO formation (m/z = 28) is noticed, which is a product of the reverse water gas shift reaction (rWGS: $CO_2 + H_2 \rightarrow CO + H_2O$) of the released CO_2 with the hydrogen feed over the pure support and the Pd modified surface. rWGS activity was also reported for pure Ga_2O_3 at temperatures above 603 K.[24] Whereas conversion of CO_2 to CO occurs at the same temperature for the Pd substituted precursors (693 K), it is delayed in case of the Pd free precursor (723 K) as illustrated in Figure S6 (left). Pd seems to promote the earlier formation of partially reduced Ga species and shifts the onset of rWGS over Ga_2O_3 to lower temperatures. In addition, for sample Pd25 traces of methane (m/z =15) are observed at 723 K, probably due to methanation of CO on the relatively large amount of metallic Pd in this sample.

XRD results of reduced catalysts:

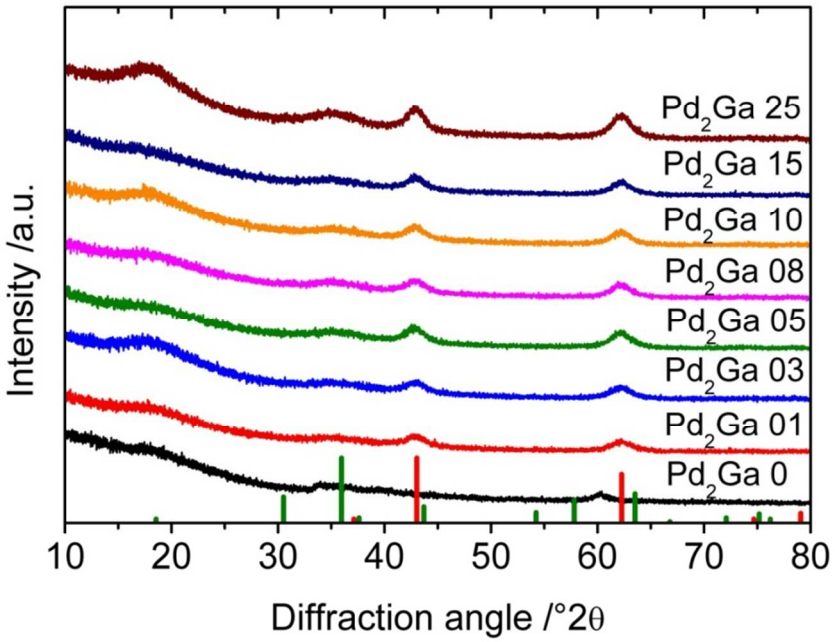

Figure S7: Powder pattern of Pd*X* samples after HTR. Red histogram corresponds to MgO (ICDD 1-1235) and the black one to $MgGa_2O_4$ (ICDD 10-113). No peaks of Pd_2Ga can be seen probably due to the low particle size.

Identification of Pd vs. Pd_2Ga by HRTEM

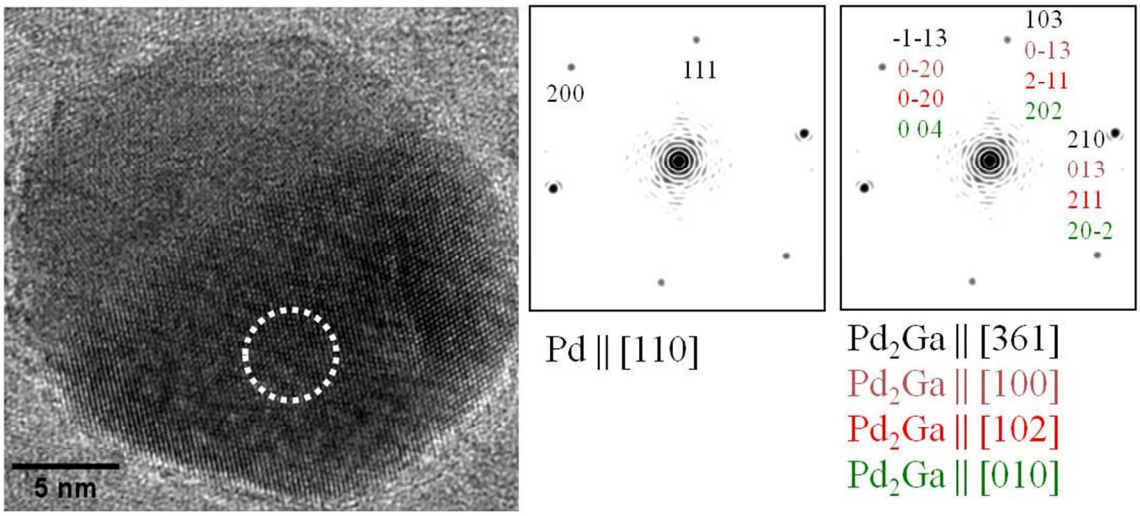

Figure S8: HRTEM image and the corresponding FFT pattern demonstrates the structural similarity of Pd and Pd_2Ga.

Pd is fcc and Pd_2Ga crystallizes in the orthorhombic space group *Pnma* with a = 5.4829(8) Å, b = 4.0560(4) Å, c = 7.7863(8) Å.[10] The phase exhibits a broad homogeneity range of 27 – 36% Ga,[11] that also can affect the exact lattice parameters. An assignment of the obtained lattice fringes to either Pd or Pd_2Ga is further complicated by the fact that different crystallographic orientations of the two structures lead to similar lattice fringe images with closely matching lattice spacing and angles between sets of lattice planes. Figure 5C and D (main article) show two cases where particles are oriented such that an

assignment can only be made to the [321] and [021] orientation of the intermetallic phase, respectively. In contrast, there are at least four different orientations of the Pd_2Ga structure for which the obtained lattice fringes and the corresponding FFT power spectra are similar to the case of Pd particles oriented along the [110] zone axis. Due to the small size of the particles and the presence of defects, the intensities of the spots in the power spectra also deviate from the theoretical values. Therefore, it is not easy to exclude the presence of Pd particles from the analysis of the electron diffraction patterns.

IR spectra of the OH-region upon CO adsorption

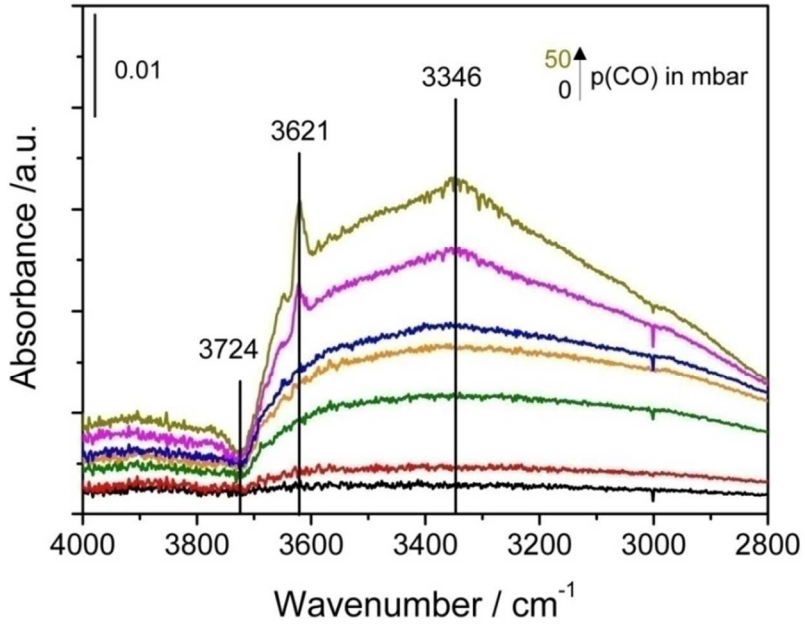

Figure S9: IR spectra of CO adsorbed on Pd10 after HTR in the OH stretching range from 4000 - 2800 cm^{-1} at RT.

Discussion of CO adsorption on Pd_2Ga nanoparticles

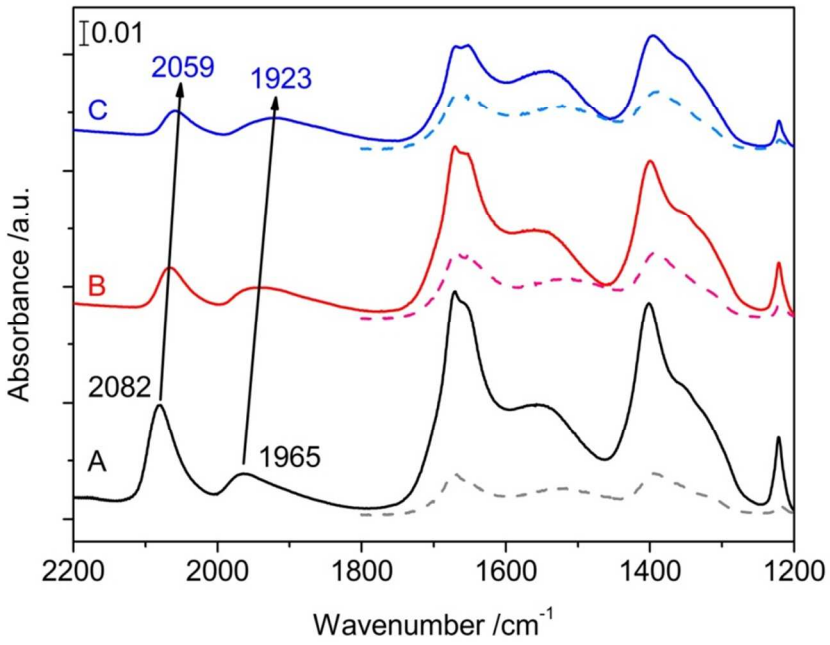

Figure S10: IR spectra of HT-reduced Pd0 (dotted) and Pd10 (straight line) after CO adsorption at RT upon evacuation: A) p_{CO} = 50mbar, t = 30min; B) p = $1.1 \cdot 10^{-5}$ mbar; C) p = $3.9 \cdot 10^{-6}$ mbar.

The desorption of CO was examined particularly with regard to determination of the active metal surface by CO chemisorption. The recorded spectra obtained after CO adsorption at a CO pressure of 50 mbar for 30 min and during evacuation to a pressure of 10^{-6} mbar are presented in Figure S10. The bands of linearly and bridged-bonded CO on Pd^0 are shifted to lower wavenumbers upon evacuation and the overall intensity decreased significantly. After complete evacuation the intensity ratio of the bands is nearly equal and typical for metallic Pd rather than for Pd_2Ga. Additionally, the formed carbonates and bicarbonates species during CO adsorption are preserved. The same behavior was also found to a minor extent for the Pd free sample (dotted lines). Consequently, we assume that major contribution of the irreversible chemisorbed CO is attributed to metallic Pd and the oxide support. The intermetallic Pd_2Ga surface only weakly adsorbs CO and decomposes in the CO atmosphere. These observations clearly complicate the interpretation of volumetric CO chemisorption data as no easy relation of irreversibly adsorbed CO with the intermetallic surface is possible.

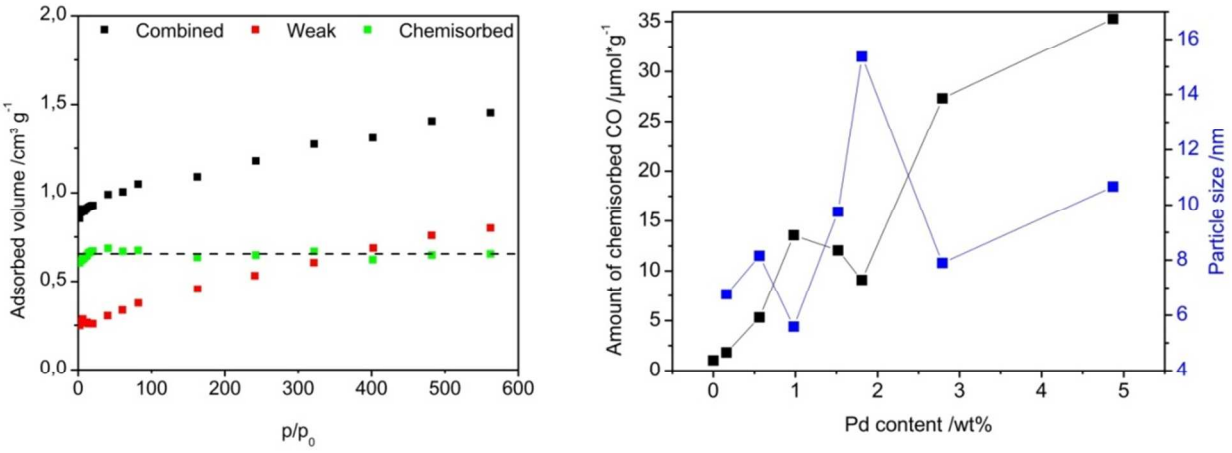

Figure S11: Combined, weak and chemisorbed isotherm of Pd25 after HTR obtain by CO chemisorption at 313 K. (bottom) The right hand panel shows the irreversible CO uptake of the sample series and the calculated corresponding particle sizes assuming Pd:CO stoichiometry of 1.5.

According to the CO-IR measurements, it is supposed that Pd_2Ga surface is partially decomposed Pd and Ga_2O_3 during chemisorption. No straight adsorption isotherm can be obtained to extrapolate the total amount and the amount of weakly adsorbed CO. No surface saturation with CO is achieved under the applied conditions and furthermore no quantification of the formed Pd patches is possible. Thus the dispersion and particle size data shown in Figure S9 are not reliable and not further considered in this work. The active surface area was determined by Dual isotherm method. The difference of combined and weak isotherm (reversible) results in the irreversible chemisorbed amount of the CO that was used for the calculation.

Catalytic data with selectivity to other products

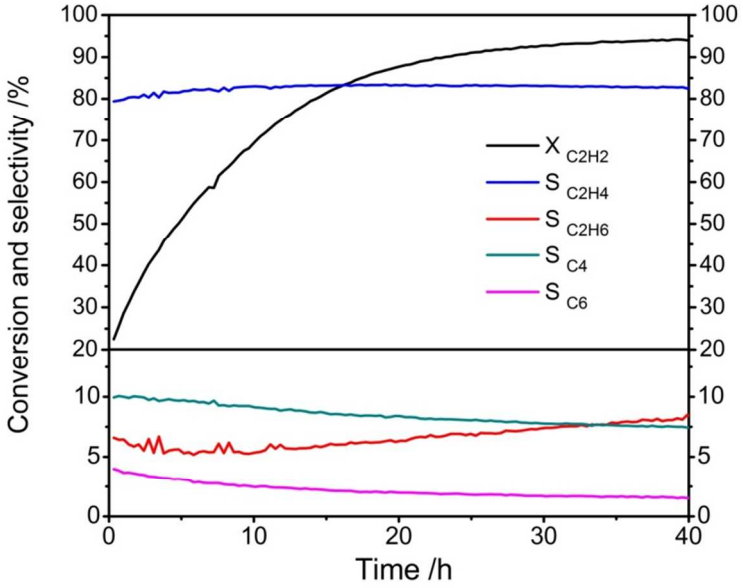

Figure S12: Conversion and selectivities at 473 K over Pd25 after HTR (100ml/min flow, 0.2 mg Pd25).

Apparent activation energy

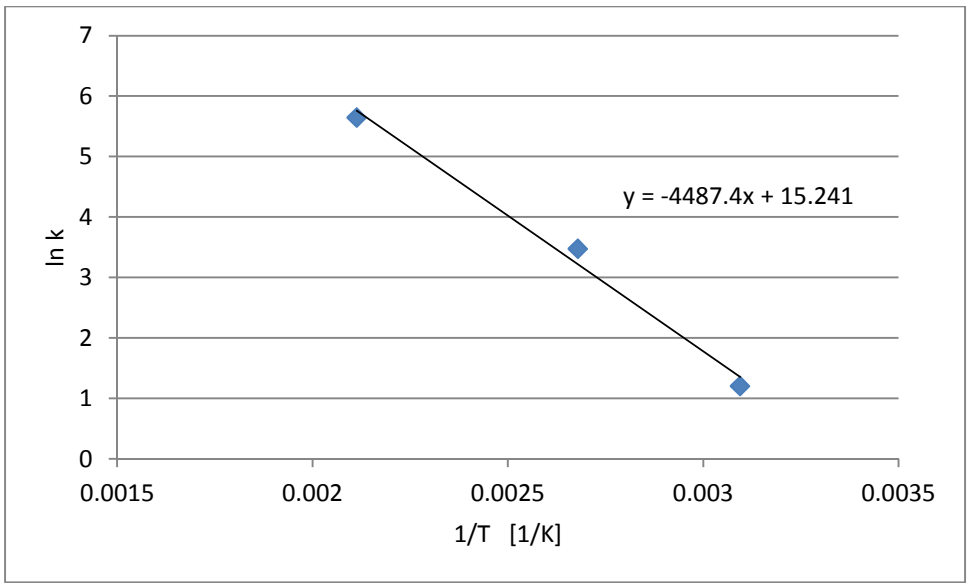

Figure S13: Arrhenius plot of catalyst Pd25

The apparent activation energy of the acetylene conversion was estimated from catalytic measurements of Pd25 at three temperatures, 473 K, 373 K and 323 K, after the reaction had reached a steady state. For the tow lower reaction temperatures 3 mg catalysts were used, while at the higher temperature 0.3 mg were used. The conversions were 85%, 97% and 10%, respectively. This data was corrected for the catalyst mass and used to estimate the apparent activation energy from the simplified Arrhenius plot shown above. The linear regression yielded a value of 37.3 kJ/mol. Significant mass transport limitations can be excluded based on the linearity of the data points.

Raman investigation of spent catalyst

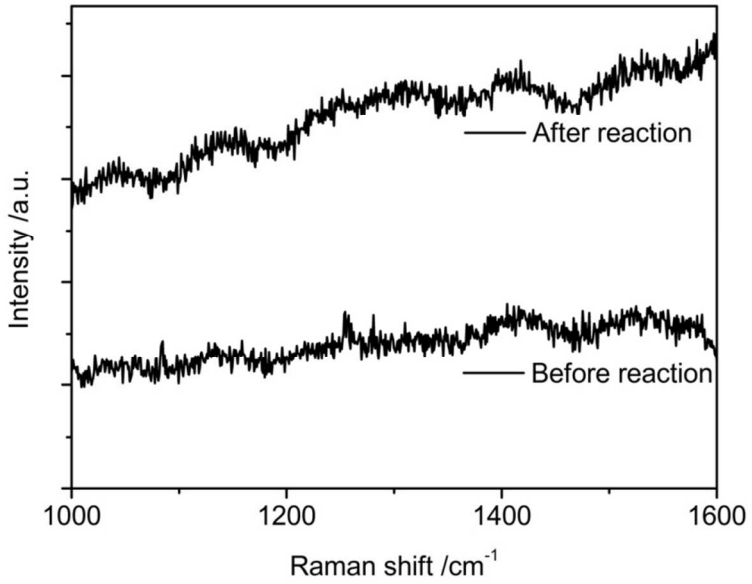

Figure S14: Raman spectra of the HT-reduced Pd25 catalyst before and after acetylene hydrogenation over 44h TOS showing no indication for amorphous carbon deposition.

TPO of spent catalyst

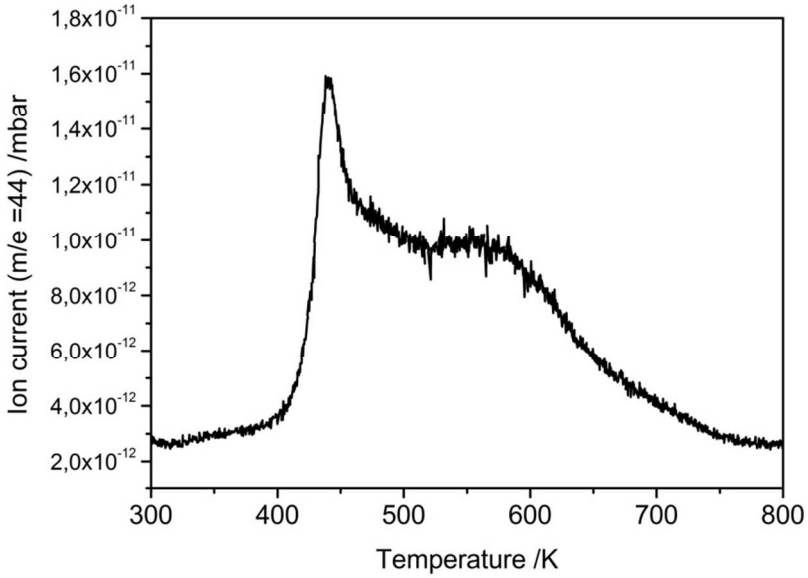

Figure S15: Temperature programmed oxidation of post-reacted Pd25 catalyst after 44h TOS in 21% O_2/Argon.

References of the supporting information material

[1] Wowsnick, G.; Teschner, D.; Kasatkin, I.; Girgsdies, F.; Armbrüster, M.; Zhang, A.; Grin, Y.; Schlögl, R.; Behrens, M. *J. Catal.* **2014**, *309*, 209.

[2] Horuiti, J.; Polanyi, M. *Trans. Farday Soc.* **1934**, *30*, 1164.

[3] Shet, P.M. ;Neurock, M.; Smith, C.M.; *J. Phys. Chem. B* **2003**, *107*, 2009.

[4] Neurock, M.; van Santen, R.A. *J. Phys. Chem. B* **2000**, *104*, 11127.

[5] Azad, S.; Kaltchev, M.; Stacciola, D.; Wu, G.; Tysoe, W.T. *J. Phys. Chem. B* **2000**, *104*, 3107.

[6] Bond, G.C.; Wells, P.B. *J. Catal.* **1965**, *5*, 65.

[7] Al-Ammar, A.S.; Webb, G. *J. Chem. Soc. Faraday Trans.* **1978**, *74*, 195.

[8] Sheppard, N.; de la Cruz, C. *Adv. Catal.* **1998**, *42*, 181.

[9] Bos, A.N.R.; Westerterp, K.R. *Chem. Emg. Proc.* **1993**, *32*, 1.

[10] Kovnir, K.; Schmidt, M.; Waurisch, C.; Armbrüster, M.; Prots, Y.; Grin, Y. *Z. Kristallogr. NCS* **2008**, *223*, 7.

[11] Okamoto, H. *J. Phase Equil. Diff.* **2008**, *29*, 466.